Inorganic Chemistry

Article

pubs.acs.org/IC

Rapid Microwave Preparation and ab Initio Studies of the Stability of the Complex Noble Metal Oxides La_2BaPdO_5 and La_2BaPtO_5

Lauren M. Misch,[†,‡] Jakoah Brgoch,[†] Alexander Birkel,[†] Thomas E. Mates,[§] Galen D. Stucky,[§,‡] and Ram Seshadri*[,§,‡]

[†]Materials Research Laboratory, University of California, Santa Barbara, California 93106, United States

[‡]Department of Chemistry and Biochemistry, University of California, Santa Barbara, California 93106, United States

[§]Materials Department, University of California, Santa Barbara, California 93106, United States

ABSTRACT: We present a rapid microwave-assisted solid-state approach to prepare complex platinum-group metal oxides with the formula La_2BaMO_5 (M = Pd, Pt). While conventional furnace-based preparations of these compounds take several days and often require oxidizing conditions, the microwave-assisted pathway enables the target compounds to be obtained with high phase purity in about 20 min of reaction time in air without the multiple regrindings that are required of conventional solid-state synthesis. These complex oxides are stable in various atmospheres up to 1000 °C unlike the simple noble metal oxides, which are reduced even at room temperature. Density functional theory-based calculations have been employed to establish the stability of these complex oxides and to understand the electronic structure origins of the stability, most notably the influence of electropositive cations. It is shown that the presence of electropositive ions in the oxide crystal structure "softens" the oxygen anion and results in more covalent (Pd/Pt)−O interactions.

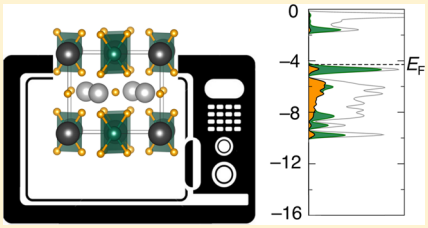

INTRODUCTION

Noble metal catalysts are widely used in many types of important reactions, ranging from automotive emissions control[1] to coupling reactions.[2] These catalysts frequently comprise noble metal nanoparticles on high surface area supports. More recently, it has been demonstrated that noble metals in their ionic forms also exhibit some catalytic reactivity, sometimes with better performance than their metallic analogs.[3] Cation-substituted materials, notably Pd-substituted perovskites,[4−7] have received considerable attention for their cost-effectiveness and utility. However, substituted materials can be challenging to prepare and are unstable under reducing reaction conditions.[8] The activity associated with noble metal ions can be accessed in complex oxides where noble metals occupy their own site in the crystal instead of substituting onto another cation site. It has also been demonstrated that pure complex oxides containing noble metals ions in unique crystallographic sites (as opposed to small substitution) can be more effective than the corresponding metallic species supported on oxides for CO oxidation.[9] Complex oxides tend to be more robust and resistant to reduction than binary oxides due to inductive effects from neighboring cations. Of particular interest in complex oxides is the potential for structure−property relationships, with the crystal structure influencing stability and resistance to reduction or degradation.

Conventional solid-state methods for preparation of complex oxides of the platinum group metals generally require extensive heating at elevated temperatures and multiple regrinding steps. Long calcination times are required because of the sluggish diffusion kinetics of (for example) Pd^{2+} in the solid state, related to the kinetic inertness of Pd^{2+} in aqueous solution.[10] The usual way to overcome sluggish diffusion is to carry out solid-state reactions at elevated temperatures. However, heating PdO or PtO at elevated temperatures results in autoreduction, even under flowing O_2,[11] and the metals are sufficiently refractory that their reoxidation is difficult. Consequently, it can take days or weeks to prepare phase-pure platinum group metal oxides using conventional furnace-heating methods. Microwave-assisted heating significantly shortens the required preparation time for phase-pure, high-quality materials. Described in the literature as early as the 1980s,[12−14] it has been shown that with simple modifications and optimizations, household microwave ovens can be employed to obtain high-quality materials, among them phosphors with high quantum yields,[15−17] intermetallics,[18,19] and other thermoelectrics.[20] The microwave heats a carbon susceptor material, which very rapidly transfers heat to the sample. Here we apply the microwave-assisted heating technique to prepare two prototypical complex oxide materials containing Pd^{2+} and Pt^{2+} and carry out a detailed analysis of their stability. Although this work focuses on microwave-assisted routes for platinum group metal oxide preparation, other methods do exist. Zur Loye and co-workers have reviewed flux growth methods for oxides such as these.[21,22]

The isostructural compounds La_2BaPdO_5 and La_2BaPtO_5 were prepared using microwave-assisted heating with the aim of accessing ionic Pd and Pt for catalytic applications. La_2BaPdO_5, previously studied by Kurzman et al. and shown to be an effective catalyst,[9] is isostructural with Y_2BaPdO_5 reported by

Received: December 6, 2013
Published: February 11, 2014

   dx.doi.org/10.1021/ic4030124 | *Inorg. Chem.* 2014, 53, 2628−2634

Laligant et al.[23] The synthesis and structure of La_2BaPtO_5 was reported by Müller-Buschbaum and Schlüter.[24]

The tetragonal structure of these complex oxides, with isolated $(Pd/Pt)O_4$ square planes, is displayed in Figure 1. The

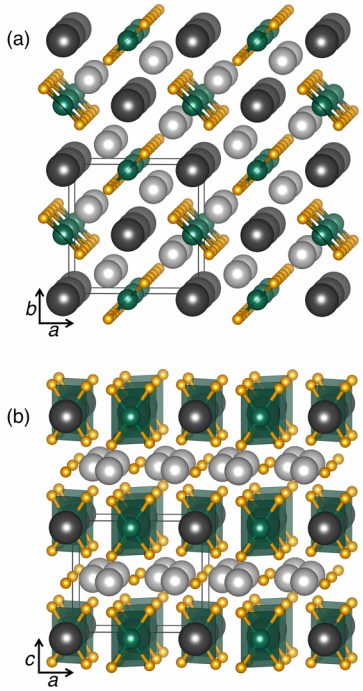

Figure 1. The crystal structure for La_2BaMO_5 (M = Pd or Pt) projected nearly down (a) the c axis and (b) the b axis. The larger dark gray spheres are Ba, the smaller light gray spheres are La. Square planes of $(Pd/Pt)O_4$ are also depicted.

compounds have been characterized using a combination of synchrotron X-ray diffraction, electron microscopy, and X-ray photoelectron spectroscopy (XPS). The reactivity/stability of the compounds have been characterized using thermogravimetric analysis under flowing H_2/N_2 (5:95%), to establish the enhanced stability of these compounds with respect to the simple oxides PdO and PtO. The formation energies have been calculated using density functional theory (DFT), and the origin of the stabilization of the complex oxides when compared with the corresponding simple oxide has been understood on the basis of DFT slab calculations following the method of van de Walle and Martin.[25] Such calculations allow the absolute energies of the different relevant states to be located and therefore compared across different systems. The results show unambiguously that on going from the simple oxides PdO or PtO to the complex counterparts La_2BaMO_5 (M = Pd, Pt), the O p states in the latter are destabilized and pushed up by the electropositive cations, which stabilizes for these oxophobic metal ions in an oxide environment.

EXPERIMENTAL METHODS

Preparation. These samples were prepared via microwave-assisted solid-state reaction pathways. For a typical synthesis of La_2BaMO_5 (M = Pd, Pt), stoichiometric amounts of La_2O_3 (heated at 700 °C overnight, 99.99%, Sigma Aldrich), M(II) acetylacetonate (M = Pd, Pt, 99% and 97% respectively, Sigma Aldrich), and $BaCO_3$ (99.95%, Alfa Aesar) were thoroughly ground in an agate mortar. A typical batch size of 250−500 mg of the mixed powder is then heated in the microwave (Panasonic NN-SN667B, 1300 W) setup, as described earlier.[15,16,18,19,26] In brief, powders of the starting materials are placed in a small dense alumina crucible that is in turn placed within a larger crucible that contains the carbon susceptor material. Both crucibles are in turn contained within an alumina fiber-board housing. A typical heating profile for both materials consisted of maximum power for between 15 and 20 min. For the phase evolution studies, the temperature was measured in various intervals during and after the reaction has finished using an infrared pyrometer (PalmerWahl DHS235XEL) aimed at the center of the inner crucible.

Characterization. Laboratory powder X-ray diffraction (XRD) data were obtained using Cu Kα radiation (Philips X'Pert) over the angular range of $15° \leq 2\theta \leq 90°$ with a step size of 0.016°. High-resolution synchrotron powder diffraction data were collected using beamline 11-BM at the Advanced Photon Source (APS), Argonne National Laboratory, using an average wavelength of 0.413893 Å. Discrete detectors covering an angular range from −6 to 16° 2θ are scanned over a 34° 2θ range, with data points collected every 0.001° 2θ at a scan speed of 0.01°/s. Full profile pattern using the LeBail[27] method and Rietveld fits[28] of the collected data were obtained using TOPAS Academic.[29] Thermogravimetric analysis (TGA) was performed using a METTLER TGA/sDTA851e ThermoGravimetric Analyzer in a temperature range between 25 and 900 °C at a heating rate of 10 °C per min. Stability of the compounds in various atmospheres (N_2, air, and H_2/N_2 (5:95%)) was monitored using a Cahn TG-2141 TGA. The samples were heated to 1100 °C with a heating ramp of 2.5 °C/min and 2 h of dwell time at the maximum temperature. X-ray photoelectron spectra were obtained on a Kratos Axis Ultra Spectrometer with monochromatic Al Kα source (E = 1486.61 eV). Samples were mounted on a stainless-steel holder, using double-sided carbon tape. The residual pressure inside the sample analysis chamber was below 7×10^{-9} Torr. Survey spectra were collected with an analyzer pass energy of 80 eV, and high-resolution Pd 3d and Pt 4f spectra were acquired at a pass energy 20 eV. Spectra were analyzed using CasaXPS software. Spectra were calibrated to the C 1s peak from adventitious hydrocarbons, expected at a binding energy of 285.0 eV. For peak fitting of the spin−orbit doublets in high-resolution scans, the $d_{3/2}$ to $d_{5/2}$ and the $f_{5/2}$ to $f_{7/2}$ peak areas were constrained to a ratio of 2/3 and 1/4, respectively. Field-emission scanning electron microscopy was performed on a FEI XL40 Sirion FEG microscope with an Oxford Inca X-ray system attached for chemical analysis. SEM samples were mounted on aluminum stubs using double-sided conductive carbon tape. The images have been recorded with an acceleration voltage of 5 kV.

Ab Initio Calculations. All ab initio calculations were performed in the framework of DFT using the Vienna ab initio Simulation Package (VASP),[30,31] in which the wave functions are described by plane-wave basis and the ionic potential is described by the projector augmented wave (PAW) method of Blöchl[32] and adapted in VASP by Kresse and Joubert.[33] Exchange and correlation was described by the Perdew−Burke−Ernzerhof generalized gradient approximation (GGA-PBE).[34] The first Brillouin zone was sampled for all reciprocal space integration using a gamma-centered 6 × 6 × 6 Monkhorst-Pack k-mesh[35] for La_2BaPdO_5, La_2BaPdO_5, and BaO, while a 8 × 8 × 4 k-mesh was used for PdO, PtO, and La_2O_3. The energy cutoff of the plane wave basis was 650 eV, with the convergence criteria set at 0.01 meV. The structures were all optimized to ensure they are in the electronic ground state. The optimized lattice parameters of La_2BaPdO_5 are a = 6.9237 Å, c = 5.9946 Å, and V = 287.37 Å^3, and for La_2BaPtO_5 they are a = 6.9456 Å, c = 5.9980 Å, and V = 289.35 Å^3, in agreement with the experimental measurement (Table 1). The optimized atomic positions are presented in Table 2 and are also in excellent agreement.

RESULTS AND DISCUSSION

Preparation and Characterization. Microwave-assisted heating allows the investigation of phase evolution and formation of materials in great detail. Samples can be rapidly heated and cooled so that characterization can be performed as the reaction proceeds. We have studied the phase evolution and formation of La_2BaMO_5 (M = Pd, Pt) on a typical La_2BaPdO_5

dx.doi.org/10.1021/ic4030124 | Inorg. Chem. 2014, 53, 2628−2634

Table 1. Rietveld Refinement and Crystal Data for La_2BaPdO_5 and La_2BaPtO_5

formula	La_2BaPdO_5	La_2BaPtO_5
radiation type, λ (Å)	synchrotron (11-BM), 0.413893	synchrotron (11-BM), 0.413893
2θ range (degree)	2.5−50	2.5−50
temperature (K)	295	295
crystal system	hexagonal	hexagonal
space group	*P*4/*mbm*	*P*4/*mbm*
lattice parameters (Å)	a = 6.8883(1)	a = 6.9353(3)
	c = 5.9296(1)	c = 5.9444(3)
volume (Å^3)	V = 281.35(1)	V = 285.91(1)
R_p (%)	7.5	11
R_{wp} (%)	9.7	14
χ^2	1.6	2.8

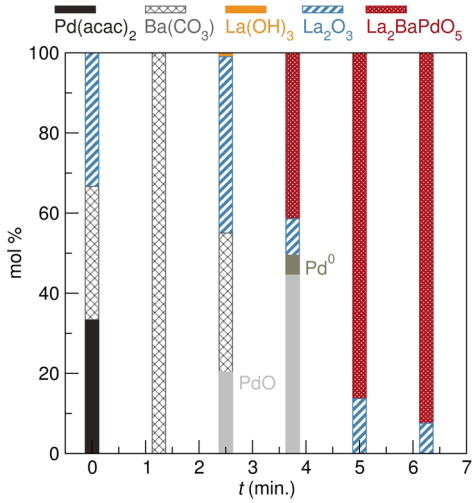

Figure 2. Phase evolution of La_2BaPdO_5 prepared by a microwave-assisted solid-state heating technique. X-ray diffraction patterns of the starting mixture and after 75 s heating intervals were taken, and Rietveld refinement revealed the mole percent of phases present. The desired phase is achieved after 3 min of reaction time and constitutes the majority of the phases present after 6 min of reaction time, as obtained from Rietveld analysis of laboratory powder X-ray diffraction data.

sample, in 75 s increments. The mole percent of phases detected by X-ray diffraction and Rietveld refinement are displayed in Figure 2. Results for the preparation of La_2BaPtO_5 were comparable.

Rietveld refinements of the starting mixture and the mixture after 75 s heating intervals reveal the mole percent of phases present at each heating step. As shown in Figure 2, the starting mixture consists only of the expected compounds that have been employed as the reactants. After 75 s of microwave heating, all precursors except the $BaCO_3$ decomposed to form an amorphous reservoir, as indicated by the background in the diffraction pattern. Another 75 s further into the reaction, PdO formed, La_2O_3 reappeared, and a small amount of $La(OH)_3$ was detected. In yet another 75 s (3:45 min of total reaction time) the final product, La_2BaPdO_5, is the majority phase in the diffraction pattern. Minor amounts of Pd^0 and PdO can be indexed in the diffraction pattern, along with some remaining La_2O_3. After 5 min at the maximum power setting, reaching peak temperatures between 1000 and 1050 °C as measured by pyrometry, only trace amounts of La_2O_3 were observed, and La_2BaPdO_5 is the majority phase. Although samples were nearly phase-pure after 5 min of reaction time, an additional 15 to 20 min of reaction, after a regrinding step time, improved the purity and crystallinity of the product. These products are described in what follows.

The final phase purity of the two complex oxides was investigated using synchrotron X-ray diffraction data. Rietveld fits are shown in Figure 3. Both samples show a high degree of phase purity, with less than 3 wt % of the secondary phase La_2O_3. The cell parameters, cell volumes, and atomic coordinates derived from the Rietveld fits using TOPAS Academic are are summarized in Tables 1 and 2. The values found here compare well to the obtained parameters found previously[24,36] on samples prepared via conventional solid-state pathways.

The presence of remaining La_2O_3 in the final product raises the question of the fate of stoichiometric amounts of Ba and Pd

Table 2. Refined Atomic Coordinates and Equivalent Isotropic Displacement Parameters of (a) La_2BaPdO_5 and (b) La_2BaPtO_5[a]

atom	Wyck. position	occ.	x	y	z	B_{eq} (Å^2)
(a) La_2BaPdO_5						
La1	4*h*	1	0.174(1) (0.176)	0.674(1) (0.676)	1/2	0.397(3)
Ba1	2*a*	1	0	0	0	0.805(5)
Pd1	2*d*	1	0	1/2	0	0.358(5)
O1	8*k*	1	0.359(1) (0.357)	0.859(1) (0.858)	0.755(1) (0.753)	0.676(3)
O2	2*b*	1	0	0	1/2	0.759(5)
(b) La_2BaPtO_5						
La1	4*h*	1	0.174(1) (0.177)	0.674(1) (0.677)	1/2	0.298(8)
Ba1	2*a*	1	0	0	0	0.83(1)
Pt1	2*d*	1	0	1/2	0	0.304(9)
O1	8*k*	1	0.361(1) (0.359)	0.861(1) (0.859)	0.751(1) (0.752)	0.84(6)
O2	2*b*	1	0	0	1/2	0.61(1)

[a]Determined by Rietveld refinement of powder synchrotron X-ray diffraction data collected at room temperature. DFT-optimized positions are provided in parentheses for comparison to the refined positions.

dx.doi.org/10.1021/ic4030124 | *Inorg. Chem.* 2014, 53, 2628−2634

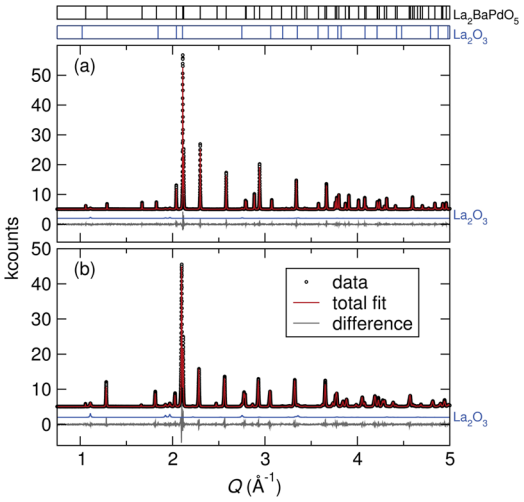

Figure 3. Synchrotron X-ray powder diffraction data of (a) La_2BaPdO_5 and (b) La_2BaPtO_5.

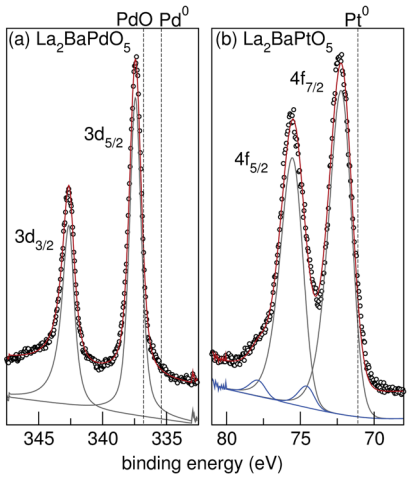

Figure 4. X-ray photoelectron spectra for the Pd 3d and Pt 4f regions in (a) La_2BaPdO_5 and (b) La_2BaPtO_5. La_2BaPtO_5 as prepared showed two doublets in the Pt 4f region, while La_2BaPtO_5 with Ar sputtering (b) showed mostly one doublet in the Pt 4f region. Ar sputtering was necessary to suppress a surface contribution from the actual bulk contribution.

precursors. To determine if the other precursors were simply evaporating off, we attempted to prepare La_2BaPdO_5 with a 5 mol % La_2O_3 deficiency. Subsequent laboratory X-ray diffraction data with Rietveld refinement did not show a significant decrease in the La_2O_3 phase present in the final product, but the formation of face-centered cubic (fcc) Pd metal was promoted. Ultimately, we expect that the Ba and Pd precursors are, in fact, still present in the final material, but are in quantities that are much less than are easily detectable. Previous work has shown that Ba readily binds hydroxyls, carbonates, and other surface species, rendering the Ba species not incorporated into the final product hard to detect by XRD.[5] Because of the lower atomic weight, Pd does not scatter as significantly as compared to La and Ba.

X-ray photoelectron spectroscopy was performed to determine the oxidation state of the Pd and Pt in La_2BaMO_5. Survey scans indicated that no elements besides the anticipated La, Ba, Pd, Pt, and O were present. Carbon was present due to sample mounting on double-sided carbon tape. The high-resolution scan of La_2BaPdO_5 showed Pd 3d peaks to be shifted to higher binding energy than Pd^0 and Pd^{2+} in PdO. This is representative of a highly ionic Pd environment. The observed peak positions and anticipated positions for the reference materials are shown in Figure 4a.

The initial high-resolution scan of La_2BaPtO_5 showed two doublets in the Pt 4f region, suggesting some surface reaction. Argon sputtering of the sample followed by another high-resolution scan, Figure 4b, of the Pt 4f region primarily showed mostly a single doublet contributing to the total signal, and a decreased contribution from the another doublet that we associate with the Pt 4f binding energy is typical of Pt^{2+} species; the shift from Pt^0 to Pt^{2+} is comparable to what is seen in the case of Pd^0 to Pd^{2+}.

The morphological features of the two complex oxides were investigated using scanning electron microscopy, and the obtained images are presented in Figure 5. Both samples, La_2BaPdO_5 and La_2BaPtO_5, exhibit comparable morphologies, with almost spherical particles and sizes ranging from 100 nm in diameter to several micrometers. The average size of the particles, derived from measurements of several hundred particles, is about 0.56 and 0.58 μm for La_2BaPdO_5 and La_2BaPtO_5, respectively. The values found from electron

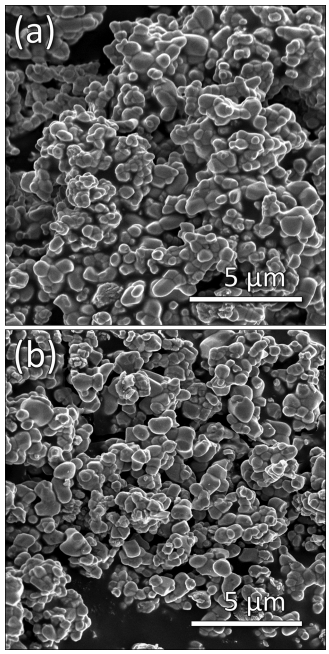

Figure 5. Scanning electron micrographs of (a) La_2BaPdO_5 and (b) La_2BaPtO_5 indicate consistent morphology and uniform particle size for samples prepared using microwave-assisted heating.

microscopy agree with the calculated crystallite sizes from the synchrotron data, about 0.4 μm. The slightly smaller size derived from the refinement might point toward the fact that the particles are not entirely single crystalline, but rather consist of several domains. It is important to note here that the crystallite and/or particle size can very easily be influenced by extending or shortening the microwave heating treatment. Energy dispersive X-ray spectroscopy and elemental mapping also indicated that ions were well-dispersed throughout the materials.

The morphology achieved for these materials prepared using microwave-assisted heating is one indicator that the microwave heating is contributing more to the materials than simply rapid

dx.doi.org/10.1021/ic4030124 | Inorg. Chem. 2014, 53, 2628−2634

heating. We expect that the dielectric loss tangents for the precursor materials used here will change as a function of temperature, and that when the precursors are heated, the sample is strongly coupling to the microwaves. This likely plays a role in the actual reaction temperature, which is measured postreaction with an infrared pyrometer. The microwave reaction pathway has been discussed in more depth previously.[12−14]

The addition of electropositive cations to the surrounding structure for noble metals will stabilize the noble metal d states.[1] With this in mind, it is likely that the Pd ions in the complex structures would reduce to Pd metal at higher temperatures than PdO. By designing a material that would maintain Pd ionicity at high temperatures even in reducing conditions, it will be adventageous when considering catalytic applications. To probe the stability with respect to decomposition at elevated temperatures, La_2BaPdO_5 and La_2BaPtO_5 were heated in flowing H_2/N_2 (5:95%) from room temperature to 1000 °C at 2.5 °C/min. The decomposition profiles are shown in Figure 6. Just before the major decomposition near

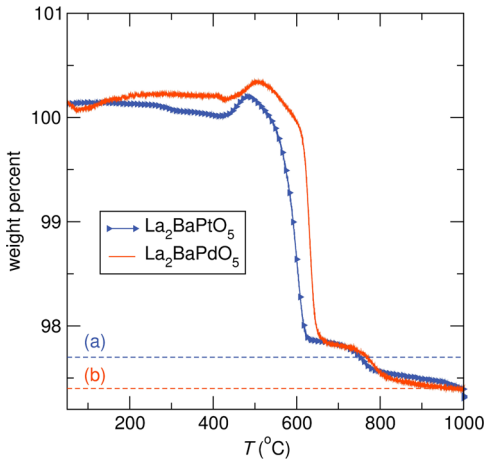

Figure 6. Thermogravmetric analysis of the decomposition of final product achieved after microwave heating. Samples were heated from room temperature to 1000 °C at 2.5 °C/min in H_2/N_2 (5:95%). La_2BaPdO_5 reduces at a slightly higher temperature than La_2BaPtO_5, and their decomposition profiles are very similar. La_2BaPdO_5 and La_2BaPtO_5 are expected to lose 2.6% and 2.3%, respectively, based on eq 2. These losses are indicated with dashed lines, (a) 2.3% for La_2BaPtO_5 and (b) 2.6% for La_2BaPdO_5, subtracted from 100%.

500 °C, an increase in mass is observed due to buoyancy effects in the TGA. At 600 °C, La_2BaPdO_5 and La_2BaPtO_5 experienced the most significant mass loss. We expect that this loss corresponds to the reduction of the Pd or Pt ion to metal with the loss of (1/2) O_2, reflected in eq 2. La_2BaPdO_5 and La_2BaPtO_5 are expected to lose 2.6% and 2.3%, respectively. These theoretical losses are indicated with dashed lines in Figure 6. La_2BaPtO_5 reduces just before the Pd analog, yet their decomposition profiles are nearly identical. For comparison, the same experiment was carried out for the binary PdO. Here, when placed under flowing H_2/N_2 (5:95%) the compound reduces readily at room temperature.

Ab Initio Studies of the Stability. The elevated temperature required to reduce the complex oxides is considerably different compared to the binary oxides, in particular PdO, which reduces at room temperature in air. To gauge the effect of structure and composition on this notable difference, the energetics of formation were calculated based on first principles. A hypothetical decomposition was considered following eqs 1 and 2, where M is Pd or Pt.

$$MO \rightarrow M + \frac{1}{2}O_2 \tag{1}$$

$$La_2BaMO_5 \rightarrow La_2O_3 + BaO + M + \frac{1}{2}O_2 \tag{2}$$

The total energy of these reactions (ΔE) at 0 K was calculated as a function of oxygen chemical potential (μ_O), using eqs 3 and 4:

$$\Delta E = E_{MO} - E_M - \mu_O - \frac{1}{2}E_{O_2} \tag{3}$$

$$\Delta E = E_{La_2BaMO_5} - E_{La_2O_3} - E_{BaO} - E_M - \mu_O - \frac{1}{2}E_{O_2} \tag{4}$$

where $E_{La_2BaMO_5}$, E_{MO}, $E_{La_2O_3}$, E_{BaO}, and E_M E_{O_2} are the total calculated energies per formula unit.

In the calculations, μ_O is the oxygen chemical potential, which varies as a function temperature and oxygen partial pressure (p) following the equation $\mu_{O_2} = E_{O_2} - kT \ln(p_0/p)$. As illustrated in Figure 7, the binary oxides are favored at

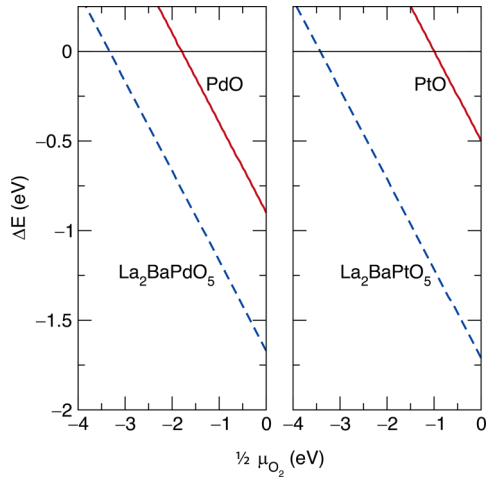

Figure 7. The energy of formation (ΔE) as a function of oxygen chemical potential (μ_O) for the reactions outlined in eqs 1 and 2. The partial pressure of oxygen is assumed to be 1×10^{-10} Pa. Temperature ranges from 0 to 1100 K.

relatively high chemical potentials of O_2 ($\mu_O < -1$ eV) but, at lower chemical potentials, display a decided preference to reduce to the metal. The equilibrium favors the complex oxides across a much wider μ_O range, and decomposition is favored only when $\mu_O < -3.5$ eV. Moreover, the decomposition of PtO occurs at a higher chemical potential, $\mu_O \approx -2.5$ eV, suggesting that the stabilization against reduction to the metal in the complex oxides is much more dramatic in La_2BaPtO_5 than it is in La_2BaPdO_5.

The origin of relative stability against decomposition for these complex oxides compared to the binary metal oxides was established from the electronic structures. To allow a direct comparison of the density of states (DOS) for PdO, PtO, La_2BaPdO_5, and La_2BaPtO_5, band offset calculations were carried out (Figure 8). Slab models were constructed using an 8

dx.doi.org/10.1021/ic4030124 | Inorg. Chem. 2014, 53, 2628−2634

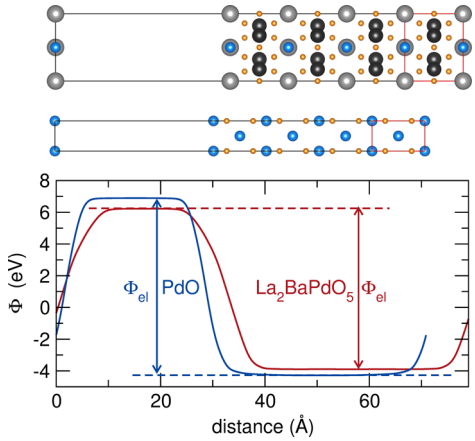

Figure 8. Band offset calculations, shown for the examples of (top) La_2BaPdO_5 and (middle) PdO were carried out to allow a direct comparison of the band positions. (bottom) Φ_{el} indicates the energy of separation between the top of the valence band and the vacuum level at 0 eV.

× 1 × 1 supercell with four cells containing the respective structures and four vacuum cells. The difference between the vacuum energy and the average electrostatic potential (Φ_{el}) is used to normalize the position of the Fermi level (E_F) for these systems. The band positions were determined by aligning the center of the vacuum region with the center of the atomic electrostatic potential (assuming it represents the bulk potential).

The DOS of La_2BaPdO_5[36] and PdO are illustrated in Figure 9, while those of La_2BaPtO_5 and PtO are shown in Figure 10.

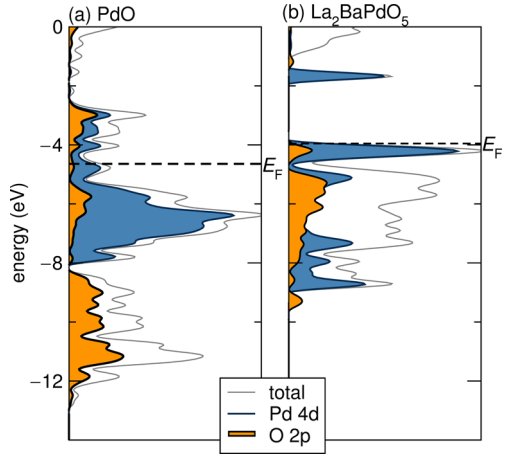

Figure 9. The calculated density of states, displayed on an absolute energy scale with reference to the vacuum level at 0 eV, for (a) PdO and (b) La_2BaPdO_5, using the PBE functional. The O 2p partial DOS corresponds to the Pd nearest neighbors. E_F is −4.64 eV for PdO and −3.95 eV for La_2BaPdO_5, relative to vacuum.

The electronic structures of the binary oxides differ significantly compared to the complex oxides. Most notably, in the case of palladium, PdO is a metal, whereas La_2BaPdO_5 is a semiconductor. However, the metallicity for PdO is an artifact due to the PBE functional. It has been shown that using a screened-hybrid functional (e.g., HSE06) opens a 1 eV gap at the Fermi level.[9] In PdO, the O 2p bands are rather disperse, with a majority of the states residing between −12 and −8 eV, while the remainder extend across E_F. The Pd 4d orbitals in PdO are

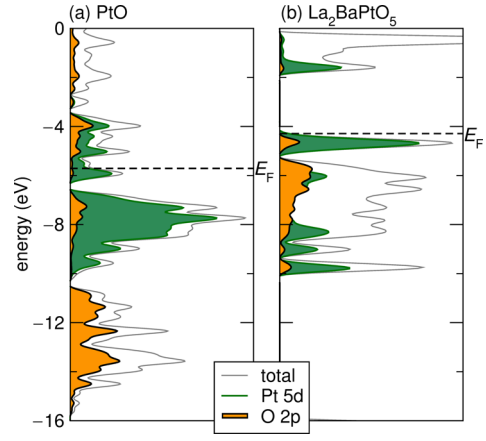

Figure 10. The calculated density of states, displayed on an absolute energy scale with reference to the vacuum level at 0 eV, for (a) PtO and (b) La_2BaPtO_5, using the PBE functional. The O 2p partial DOS corresponds to the Pd nearest neighbors. E_F is −5.71 eV for PtO and −4.29 eV for La_2BaPtO_5, relative to vacuum.

fairly narrow between −8 to −3 eV. The complex oxide La_2BaPdO_5 has a wider band gap (∼2 eV) compared to the binary oxide, with the valence band maximum (VBM) composed of Pd 4d states and the conduction band minimum (CBM) coming from the O 2p states. The Pd 4d states span from −7 eV to the E_F, while the O 2p orbitals are higher in energy compared to PdO, showing nearly perfect energetic overlap with the Pd 4d orbitals. The DOS of the Pt oxides are nearly identical to the Pd oxides. In PtO, the compound is also calculated to be a metal, although using a hybrid functional will open a gap.[37] The O 2p orbitals span a wider energy range, from −16 eV to above E_F, with a majority of the states between −16 and −10 eV. The Pt 5d orbitals have nearly the same band dispersion as PdO, extending from approximately −10 to −4 eV. La_2BaPtO_5 also has a similar electronic structure to the Pd analogue. The O 2p bands range between −10 eV and E_F as well as above −2 eV composing the CBM. The Pt 5d orbitals are in the same energy region, between −10 eV and E_F, and make up the VBM.

The changes in the DOS going from the binary oxide to the complex oxide are due to the incorporation of the more electropositive cations in the structure (i.e., Ba^{2+} and La^{3+}).[1] Adding the unoccupied orbitals of these cations destabilizes the oxygen 2p states, raising their energy, as observed in Figures 9 and 10. Increasing the energy of the O 2p states to the same energy window as the transition metal promotes orbital overlap of the *M*−O square planes. These changes in electronic structure suggest a pathway for the stabilization of these complex oxides with respect to reduction.

■ CONCLUSIONS

La_2BaPdO_5 and La_2BaPtO_5 were prepared using microwave-assisted heating. X-ray diffraction indicated that the desired phase was present after just a few minutes and that highly crystalline materials could be achieved after 20 min of heating. This represents significant savings in time, compared to conventional solid-state methods, that can take days or weeks of heating. Confirmed by XPS and TGA, these materials stabilize ionic Pd^{2+} and Pt^{2+} and maintain their ionic nature up to 600 °C under H_2/N_2 (5:95%). The stability of Pd^{2+} and Pt^{2+} ions is directly related to the introduction of electropositive cations into the surrounding lattice. Electronic structure

dx.doi.org/10.1021/ic4030124 | Inorg. Chem. 2014, 53, 2628−2634

calculations using DFT, of the energies of formation and of the absolute energetics of electronic states support such stabilization and provide credence for the hypothesis that O-p states, are shifted up in energy with the introduction of these cations, to contribute to increased covalency of O p with noble metal d states.

AUTHOR INFORMATION

Corresponding Author

*E-mail: seshadri@mrl.ucsb.edu.

Notes

The authors declare no competing financial interest.

ACKNOWLEDGMENTS

This work was supported by the Department of Energy through DE-FG02-10ER16081. L.M.M. acknowledges support from the ConvEne IGERT Program (NSF-DGE 0801627) and thanks Alan R. Derk for helpful discussion. The research carried out here made extensive use of shared experimental facilities of the Materials Research Laboratory: the MRL Central Facilities are supported by the MRSEC Program of the NSF under Award No. DMR 1121053; a member of the NSF-funded Materials Research Facilities Network (www.mrfn.org). We also gratefully acknowledge the UCSB Center for Scientific Computing, supported by the California Nanosystems Institute (NSF CNS-0960316), Hewlett-Packard, and the Materials Research Laboratory. We thank Dr. Christina Birkel for the help with the TGA analysis. Use of the Advanced Photon Source at Argonne National Laboratory was supported by the U.S. Department of Energy, Office of Science, Office of Basic Energy Sciences, under Contract No. DE-AC02-06CH11357.

REFERENCES

(1) Kurzman, J. A.; Misch, L. M.; Seshadri, R. *Dalton Trans.* **2013**, *42*, 14653−14667.
(2) Misch, L.; Birkel, A.; Figg, C. A.; Fors, B. P.; Stucky, G. D.; Hawker, C. J.; Seshadri, R. *Dalton Trans.* **2013**, *43*, 2079−2087.
(3) Hegde, M. S.; Madras, G.; Patil, K. C. *Acc. Chem. Res.* **2009**, *42*, 704−712.
(4) Nishihata, Y.; Mizuki, J.; Akao, T.; Tanaka, H.; Uenishi, M.; Kimura, M.; Okamoto, T.; Hamada, N. *Nature* **2002**, *418*, 164−167.
(5) Li, J.; Singh, U. G.; Bennett, J. W.; Page, K.; Weaver, J. C.; Zhang, J.-P.; Proffen, T.; Rappe, A. M.; Scott, S.; Seshadri, R. *Chem. Mater.* **2007**, *19*, 1418−1426.
(6) Li, J.; Singh, U. G.; Schladt, T. D.; Stalick, J. K.; Scott, S. L.; Seshadri, R. *Chem. Mater.* **2008**, *20*, 6567−6576.
(7) Singh, U.; Li, J.; Bennett, J.; Rappe, A.; Seshadri, R.; Scott, S. *J. Catal.* **2007**, *249*, 349−358.
(8) Misch, L. M.; Kurzman, J. A.; Derk, A. R.; Kim, Y.-I.; Seshadri, R.; Metiu, H.; McFarland, E. W.; Stucky, G. D. *Chem. Mater.* **2011**, *23*, 5432−5439.
(9) Kurzman, J. A.; Miao, M.-S.; Seshadri, R. *J. Phys.: Condens. Matter* **2011**, *23*, 465501.
(10) Greenwood, N. N.; Earnshaw, A. *Chemistry of the Elements*, 2nd ed.; Butterworth-Heinemann; Oxford, U.K., 1997; pp 1144−1172.
(11) Peuckert, M. *J. Phys. Chem.* **1985**, *89*, 2481−2486.
(12) Roy, R.; Komarneni, S.; Yang, L. *J. Am. Ceram. Soc.* **1985**, *68*, 392−395.
(13) Katz, J. D. *Annu. Rev. Mater. Sci.* **1992**, *22*, 153−170.
(14) Baghurst, D.; Chippindale, A.; Mingos, D. M. P. *Nature* **1988**, *332*, 311.
(15) Birkel, A.; Darago, L. E.; Morrison, A.; Lory, L.; George, N. C.; Mikhailovsky, A. A.; Birkel, C. S.; Seshadri, R. *Solid State Sci.* **2012**, *14*, 739−745.
(16) Birkel, A.; Denault, K. A.; George, N. C.; Doll, C. E.; He, B.; Mikhailovsky, A. A.; Birkel, C. S.; Hong, B.-C.; Seshadri, R. *Chem. Mater.* **2012**, *24*, 1198−1204.
(17) Birkel, A.; DeCino, N. A.; George, N. C.; Hazelton, K. A.; Hong, B.-C.; Seshadri, R. *Solid State Sci.* **2013**, *19*, 51−57.
(18) Birkel, C. S.; Zeier, W. G.; Douglas, J. E.; Lettiere, B. R.; Mills, C. E.; Seward, G.; Birkel, A.; Snedaker, M. L.; Zhang, Y.; Snyder, G. J.; Pollock, T. M.; Seshadri, R.; Stucky, G. D. *Chem. Mater.* **2012**, *24*, 2558−2565.
(19) Birkel, C. S.; Douglas, J. E.; Lettiere, B. R.; Seward, G.; Verma, N.; Zhang, Y.; Pollock, T. M.; Seshadri, R.; Stucky, G. D. *Phys. Chem. Chem. Phys.* **2013**, *15*, 6990−6997.
(20) Biswas, K.; Muir, S.; Subramanian, M. *Mater. Res. Bull.* **2011**, *46*, 2288−2290.
(21) Mugavero, S. J. I.; Gemmill, W. R.; Roof, I. P.; Zur Loye, H. C. *J. Solid State Chem.* **2009**, *182*, 1950−1963.
(22) Bugaris, D. E.; Zur Loye, H. C. *Angew. Chem., Int. Ed.* **2012**, *51*, 3780−3811.
(23) Laligant, Y.; Ferey, G.; Hervieu, M.; Raveau, B. *Eur. J. Solid State Inorg. Chem.* **1988**, *25*, 111−117.
(24) Müller-Buschbaum, H.-K.; Schlüter, D. *J. Less-Common Met.* **1990**, *166*, L7−L0.
(25) Van de Walle, C. G.; Martin, R. M. *Phys. Rev. B* **1986**, *34*, 5621−5634.
(26) Ramesh, P. D.; Brandon, D.; Schächter, L. *Mater. Sci. Eng., A* **1999**, *266*, 211−220.
(27) Le Bail, A.; Duroy, H.; Fourquet, J. *Mater. Res. Bull.* **1988**, *23*, 447−452.
(28) Rietveld, H. M. *J. Appl. Crystallogr.* **1969**, *2*, 65−71.
(29) Coelho, A. A. *Topas Academic,* V4.1; Software, Coelho Software: Brisbane, Australia, 2007.
(30) Kresse, G.; Furthmuller, J. *Phys. Rev. B* **1993**, *47*, 558−561.
(31) Kresse, G.; Furthmuller, J. *Phys. Rev. B* **1996**, *54*, 11169−11186.
(32) Blöchl, P. *Phys. Rev. B* **1994**, *50*, 17953−17979.
(33) Kresse, G.; Joubert, D. *Phys. Rev. B* **1999**, *59*, 1758−1775.
(34) Perdew, J.; Burke, K.; Ernzerhof, M. *Phys. Rev. Lett.* **1996**, *77*, 3865−3868.
(35) Monkhorst, H. J.; Pack, J. D. *Phys. Rev. B* **1976**, *13*, 5188−5192.
(36) Kurzman, J. A.; Ouyang, X.; Im, W. B.; Li, J.; Hu, J.; Scott, S. L.; Seshadri, R. *Inorg. Chem.* **2010**, *49*, 4670−4680.
(37) Uddin, J.; Peralta, J. E.; Scuseria, G. E. *Phys. Rev. B* **2005**, *71*, 155112.